SCIENTIFIC REPORTS
nature research

Check for updates

OPEN

First-principles investigation of $LaMg_2Ni$ and its hydrides

Weiqing Jiang[1]✉, Yujie Chen[1], Xiaohua Mo[2] & Xinglang Li[1]

Using first-principles density functional theory calculations, the electronic structures of $LaMg_2Ni$ and its hydrides $LaMg_2NiH_{4.5}$ (intermediate phase) and $LaMg_2NiH_7$ (fully hydrogenated phase), as well as the H adsorption on $LaMg_2Ni$ (100) surface were investigated. For comparision, the atomic bonding characteristics of Co- and Pd-doped $LaMg_2Ni$, $LaMg_2NiH_{4.5}$ and $LaMg_2NiH_7$ compounds were also studied. Our aim is to provide new insights into the hydrogenation of $LaMg_2Ni$. The results show that the metallic intermediate hydride $LaMg_2NiH_{4.5}$ with Ni–H covalent bonds may act as the precursor state from the host compound $LaMg_2Ni$ to the full hydride $LaMg_2NiH_7$. Upon $LaMg_2Ni$ hydrogenation, the suppression of Mg–Ni and Ni–H interactions as well as the formation of La-H bonds favors for $LaMg_2Ni$–H formation.

Hydrogen is an ideal energy carrier, but a major challenge in a future "hydrogen economy" is to develop a safe, efficient and compact hydrogen storage technology. Usually, there are three methods used to store hydrogen, including gas compression, cryogenic liquid storage, and solid state hydrogen storage. Among them, solid state hydrogen storage can offer increased hydrogen density in a safe way[1].

Magnesium-based alloys are considered to be one promising materials for solid state hydrogen storage due to high storage capacity, abundant resources of magnesium and low cost[2–5]. A typical example is Mg_2Ni, which can be easily synthesized by combination Mg and Ni, and reacts readily with gaseous hydrogen at moderate temperatures and pressures to form a reversible hydride Mg_2NiH_4 containing 3.8 wt% hydrogen[6]. However, the slow absorption/desorption kinetics and the high thermodynamical stability of its hydride severely limit the practical application of Mg_2Ni[7–10]. It was reported that an improved absorption conditions can be obtained by alloying Mg_2Ni and rare earth elements to form ternary alloys such as $LaMg_2Ni$, as the rare earth hydride (La–H) can effectively catalyze hydriding reactions[8,11–13]. For example, Ouyang et al.[11] compared pure Mg_2Ni with $LaMg_2Ni$ on both thermodynamics and kinetics, and found that $LaMg_2Ni$ not only has a lower ΔH (− 51 kJ/mol H_2) and ΔS (− 105 J/K mol H_2) for hydriding reaction, compared to the ΔH (− 65 kJ/mol H_2) and ΔS (− 122 J/K mol H_2) for pure Mg_2Ni, but also costs less time to reach the saturated hydrogen capacity at lower temperature (1,100 s at 561 K for $LaMg_2Ni$ vs. 1,800 s at 573 K for Mg_2Ni[14]). This leads to a decreased hydride stability and an enhanced hydriding kinetics for $LaMg_2Ni$, and is ascribed to the presence of $LaH_{2.46}$. Zhao et al.[12] investigated the hydrogen storage properties of Mg_2Ni + x wt% $LaMg_2Ni$ (x = 0, 10, 20, 30) composites, and showed that the existence of LaH_3 phase contributed to a significant improvement in reversible hydrogen storage properties of the composites over Mg_2Ni at low temperature. Pei et al.[13] studied the phase structures and hydrogen storage properties of RMg_2Ni (R = La, Ce, Pr, Nd) alloys, and reported that the rare earth hydrides (R–H) in the alloys was helpful to improve the thermodynamic properties and accelerate the hydriding kinetics.

In recent years, the ternary compound $LaMg_2Ni$ which has better hydrogen storage properties than pristine binary compound Mg_2Ni has attracted considerable attention. Lots of works focus on the hydrogenation/dehydrogenation of $LaMg_2Ni$, and verify the facts that the intermetallic compound $LaMg_2Ni$ absorbs hydrogen reversibly near ambient conditions hereby forming a fully hydrogenated phase $LaMg_2NiH_7$ with $LaMg_2NiH_{4.6}$/$LaMg_2NiH_{4.5}$ as intermediate phase; the intermediate phase $LaMg_2NiH_{4.6}$/$LaMg_2NiH_{4.5}$ plays an important role in $LaMg_2Ni$–H ($LaMg_2Ni$ hydride) system; the La–H hydrides formed upon hydrogenation shows good catalytic effect on hydriding/dehydriding reactions of $LaMg_2Ni$; and the catalysts addition effectively modifies the hydrogen storage performance of $LaMg_2Ni$[8,11–13,15–20]. Nevertheless, the hydrogen storage mechanisms of $LaMg_2Ni$ are still not properly understood. In the present works, the theoretical studies on the electronic structure of $LaMg_2Ni$ and its hydrides (intermediate phase $LaMg_2NiH_{4.5}$ and fully hydrogenated phase $LaMg_2NiH_7$) in comparison with

[1]School of Physical Science & Technology, Guangxi Key Laboratory for Electrochemical Energy Materials, Guangxi University, Nanning 530004, China. [2]School of Mathematics and Physics, Key Laboratory for Ionospheric Observation and Simulation, Guangxi University for Nationalities, Nanning 530006, China. ✉email: wqjiang@gxu.edu.cn

corresponding Co- and Pd-containing compounds based on first-principles density functional theory calculations, should be of great interest, since Co and Pd can drastically reduce the reaction time for $LaMg_2Ni$-H hydride formation[20]. As in previous studies, Co/Pd was reported to predominantly occupy La/Ni position in $LaMg_2Ni$, respectively[20]. Here, Co-containing compounds ($LaMg_2Ni$–Co, $LaMg_2NiH_{4.5}$–Co and $LaMg_2NiH_7$–Co) are introduced by single-substitution of one Co atom at La site in $LaMg_2Ni$, $LaMg_2NiH_{4.5}$ and $LaMg_2NiH_7$, respectively. Similarly, Pd-containing compounds ($LaMg_2Ni$–Pd, $LaMg_2NiH_{4.5}$–Pd and $LaMg_2NiH_7$–Pd) are designed with Pd substitution for Ni. In addition, to further understand the hydrogenation of $LaMg_2Ni$, the hydrogen adsorption on $LaMg_2Ni$ (100) surface is also studied.

Computational details

Theoretical calculations were carried out using density functional theory (DFT) as implemented in Cambridge Serial Total Energy Package (CASTEP) code[21]. The exchange–correlation function was treated by the generalized gradient approximation of Perdew–Wang 91 (GGA-PW91)[22]. The ultrasoft pseudopotentials with valence states $5s^25p^65d^16s^2$ for La, $2p^63s^2$ for Mg, $3d^84s^2$ for Ni and $1s^1$ for H were used to describe the core electrons. A plane-wave cutoff energy of 800 eV, and a Monkhorst–Pack k-point mesh of $4\times3\times2$ for $LaMg_2Ni$ systems ($LaMg_2Ni$, $LaMg_2Ni$–Co, $LaMg_2Ni$–Pd), $2\times2\times2$ for $LaMg_2NiH_{4.5}$ systems ($LaMg_2NiH_{4.5}$, $LaMg_2NiH_{4.5}$–Co, $LaMg_2NiH_{4.5}$–Pd), and $2\times4\times2$ for $LaMg_2NiH_7$ systems ($LaMg_2NiH_7$, $LaMg_2NiH_7$–Co, $LaMg_2NiH_7$–Pd) were adopted for our calculations. Structural relaxations were carried out by Broyden–Fletcher–Goldfarb–Shanno (BFGS) method[23] until the residual forces, stresses and displacement were less than 0.03 eV/Å, 0.05 GPa and 0.001 Å, respectively.

In general, the intermetallic compound $LaMg_2Ni$ crystallizes in orthorhombic structure with space group Cmcm and lattice parameters a = 4.227 Å, b = 10.303 Å, c = 8.36 Å[15]. Hydrogenation of $LaMg_2Ni$ at near ambient conditions leads to the formation of intermediate phase $LaMg_2NiH_{4.6}$/$LaMg_2NiH_{4.5}$ before the completion of $LaMg_2NiH_7$. Here, the intermediate phase $LaMg_2NiH_{4.5}$ (space group P21/m and lattice parameters a = 8.602 Å, b = 7.937 Å, c = 6.114 Å, β = 99.53[017]) is selected for our calculations, because the model structure of $LaMg_2NiH_{4.5}$, which reproduces the powder neutron diffraction (PND) pattern without significant loss of fitting accuracy, can meet with the requirements of computational symmetry, furthermore, the crystallographic parameters of $LaMg_2NiH_{4.5}$ predicted using DFT calculations are in good agreement with those of $LaMg_2NiH_{4.6}$ determined from PND experiment[17]. The hydride $LaMg_2NiH_7$ has monoclinic structure with space group P21/c and lattice parameters a = 13.979 Å, b = 4.703 Å, c = 16.025 Å, β = 125.24[015]. Geometry optimizations of lattice constants and atomic positions on bulk $LaMg_2Ni$, $LaMg_2NiH_{4.5}$ and $LaMg_2NiH_7$ gained the relaxed crystals. Calculations for bulk $LaMg_2Ni$, $LaMg_2NiH_{4.5}$ and $LaMg_2NiH_7$ were performed using the relaxed $1\times2\times1$ (Fig. 1a), $1\times2\times1$ supercells (Fig. 1b) and primary cell (Fig. 1c), respectively, to ensure all studied systems with the same number of La, Mg and Ni atoms and make the computational results more comparable. In $LaMg_2Ni$, $LaMg_2NiH_{4.5}$ and $LaMg_2NiH_7$ crystals (Fig. 1), partial La (marked with S1) and Ni atoms (marked with S2) are substituted by Co and Pd respectively to introduce Co- and Pd-doped compounds $LaMg_2Ni$–Co, $LaMg_2NiH_{4.5}$–Co, $LaMg_2NiH_7$–Co, $LaMg_2Ni$–Pd, $LaMg_2NiH_{4.5}$–Pd and $LaMg_2NiH_7$–Pd. A structure of $LaMg_2Ni$ (100) surface was built from the optimized $LaMg_2Ni$ $1\times2\times1$ bulk structure (Fig. 1a), which consisted of three La–Mg–Ni layers with 48 atoms (12 La, 24 Mg and 12 Ni). The vacuum space in the surface is 15 Å along the z direction. It is generally believed that H atom can interact with La atom to form La-H hydride upon $LaMg_2Ni$ hydrogenation[8,11–13], and Ni atom on La-Ni alloy surface has good catalysis on the surface activity and the initial steps of hydrogen storage (hydrogen adsorption and dissociation)[24–26]. For these facts, here, the initial positions of H on $LaMg_2Ni$ (100) surface is on the bridge site of La-Ni atoms, the top site of La atom and the top site of Ni atom, as shown in Fig. 2. The initial distances between the adsorbed H atom and the considered La/Ni atom are also described in Fig. 2. During the structural optimization of surface model, all atoms in the top two layers were allowed to relax, whereas the atoms in the bottom one layer were fixed.

Results and discussion

Geometry optimization. In our studies, geometry optimizations on bulk $LaMg_2Ni$, $LaMg_2NiH_{4.5}$, $LaMg_2NiH_7$ and their corresponding Co- and Pd-containing compounds ($LaMg_2Ni$–Co, $LaMg_2NiH_{4.5}$–Co, $LaMg_2NiH_7$–Co, $LaMg_2Ni$–Pd, $LaMg_2NiH_{4.5}$–Pd and $LaMg_2NiH_7$–Pd) provided the optimized lattice parameters and cell volume shown in Table 1. As can be seen, the agreement between the optimized results and the available literature values[15,17,20] is fairly good. This suggests that the present calculations for bulk compounds are highly reliable[27]. Structural relaxations on H-adsorbed $LaMg_2Ni$ (100) systems results the relaxed La–H and Ni–H distances listed in Table 2. It is found that H adsorption on $LaMg_2Ni$ (100) surface extends La–H distance, but shortens the Ni–H distance, as compared with their initial distances (Fig. 2). And this extended La–H distance is close to that in LaH_3 hydride (2.43 Å[16]).

Thermal stability. In general, the formation enthalpy ΔH can be used to evaluate the thermal stability of considered compound. A negative formation enthalpy shows an exothermic process. Furthermore, a lower formation enthalpy implies a stronger stability[28]. Here, based on the hydrogenation reaction from $LaMg_2Ni$ to $LaMg_2NiH_{4.5}$ (Reaction 1) and $LaMg_2NiH_7$ (Reaction 2), the formation enthalpy for $LaMg_2NiH_{4.5}$ (ΔH_1) and $LaMg_2NiH_7$ (ΔH_2) are calculated by the Eqs. (3) and(4), respectively.

$$LaMg_2Ni + \frac{9}{4}H_2 \rightarrow LaMg_2NiH_{4.5} \quad (1)$$

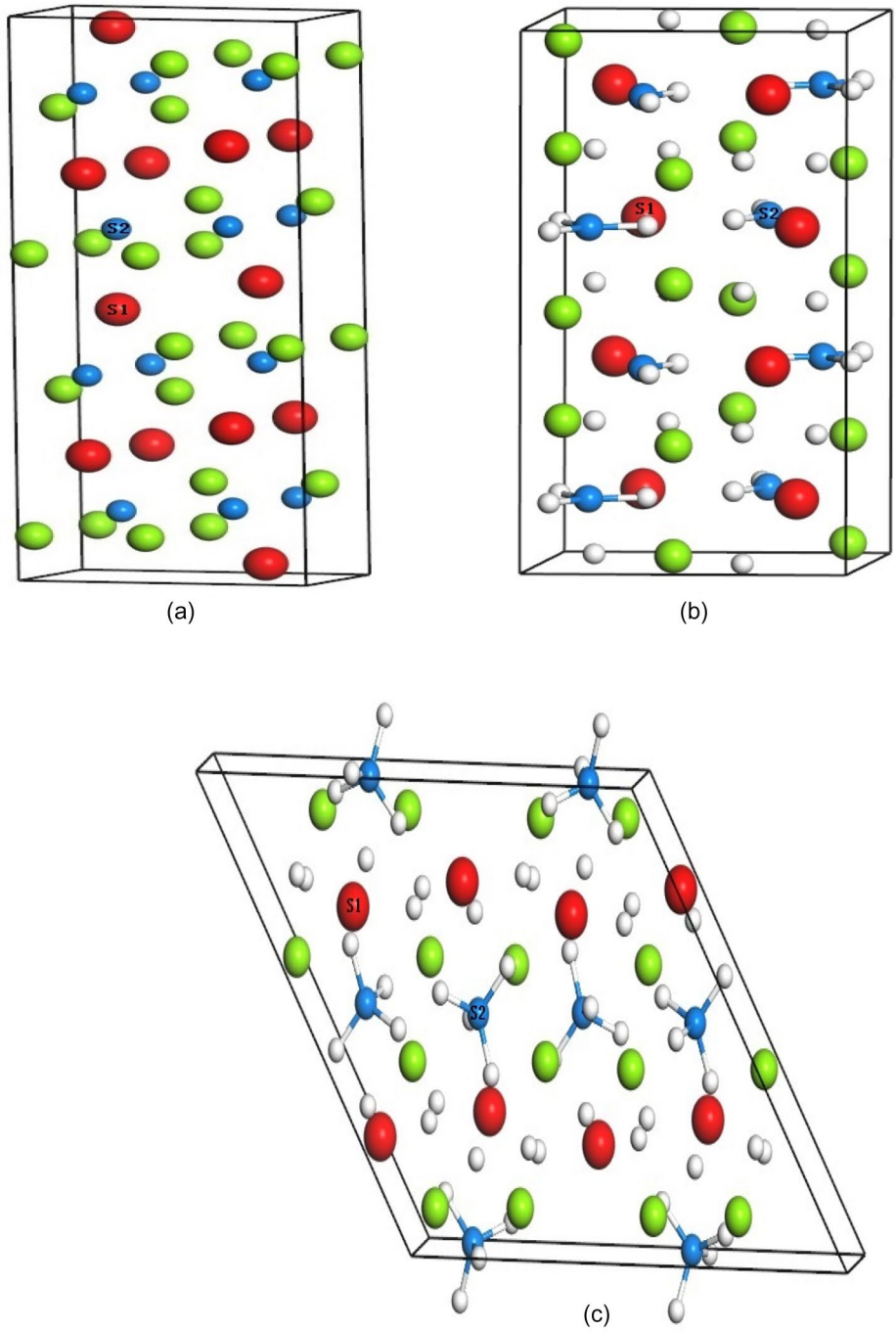

Figure 1. Model of the crystal structure, (**a**) $LaMg_2Ni$ with $1\times2\times1$ supercell; (**b**) $LaMg_2NiH_{4.5}$ with $1\times2\times1$ supercell; (**c**) $LaMg_2NiH_7$ with primitive cell. Red, green, blue and white spheres denote La, Mg, Ni and H atoms, respectively. S1 and S2 represent substitution sites of La and Ni, respectively.

$$LaMg_2Ni + \frac{7}{2}H_2 \rightarrow LaMg_2NiH_7 \tag{2}$$

$$\Delta H_1 = \frac{4}{9} \times \left[E(LaMg_2NiH_{4.5}) - E(LaMg_2Ni) - \frac{9}{4}E(H_2)\right] \tag{3}$$

$$\Delta H_2 = \frac{2}{7} \times \left[E(LaMg_2NiH_7) - E(LaMg_2Ni) - \frac{7}{2}E(H_2)\right] \tag{4}$$

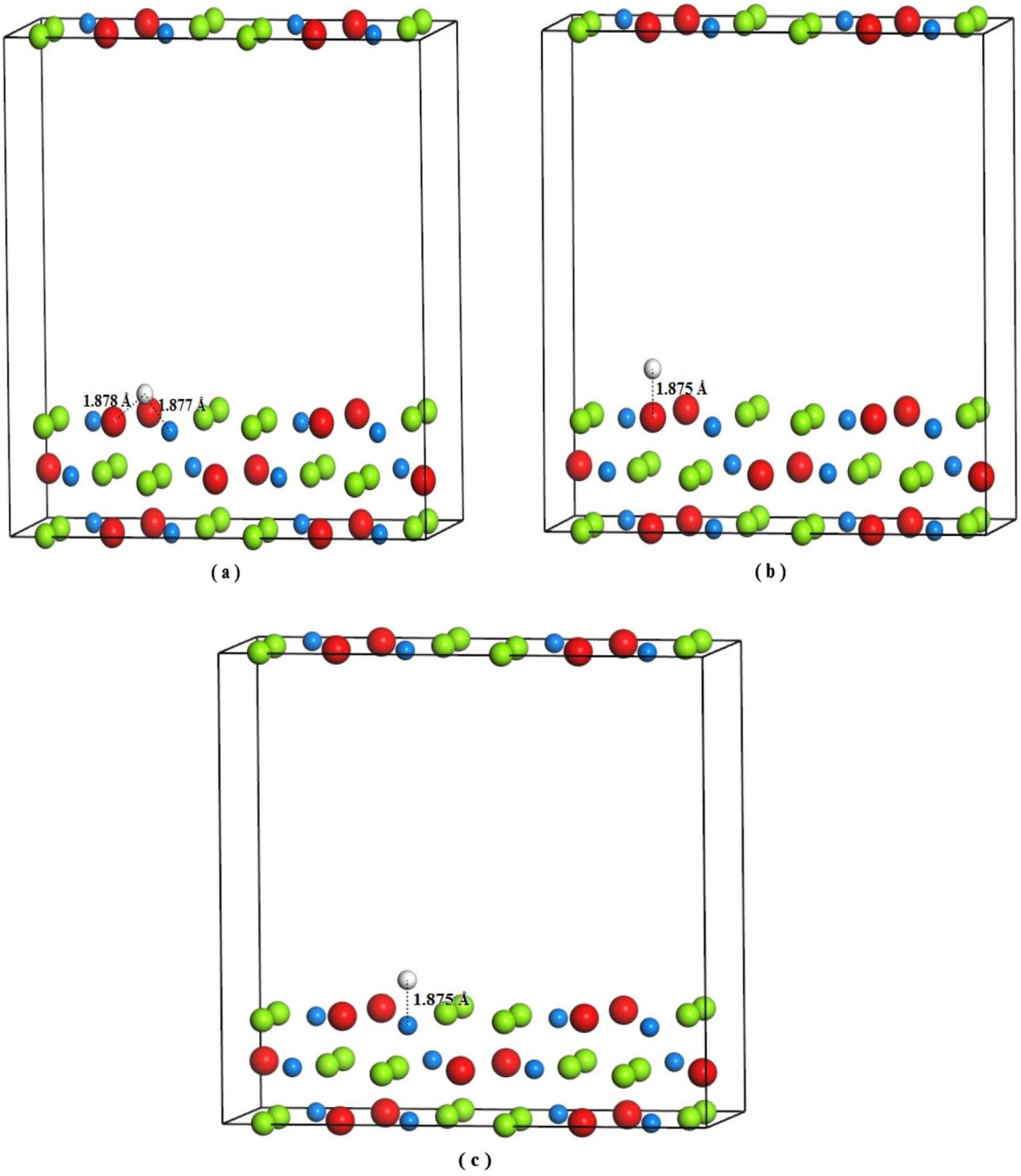

Figure 2. Model of $LaMg_2Ni$ (100) surface with H adsorbed on the bridge site of La–Ni atoms (**a**), the top site of La atom (**b**) and the top site of Ni atom (**c**). Red, green, blue and white spheres denote La, Mg, Ni and H atoms, respectively. Numbers in the figure are the initial La–H and/or Ni–H distances.

In Eqs.(3) and (4), E is the total energy of corresponding systems, which is − 4,169.875, − 4,243.606 and − 4,284.289 eV for $LaMg_2Ni$, $LaMg_2NiH_{4.5}$ and $LaMg_2NiH_7$, respectively. $E(H_2)$, the energy of hydrogen molecule, is estimated to be − 31.79 eV using a 1,000 $Å^3$ cubic unit cell containing two H atoms 0.741 Å apart[29], and the result agrees well with the literature report of − 31.592 eV[30]. The calculated formation enthalpy for $LaMg_2NiH_{4.5}$ ($\Delta H_1 = -94.46$ kJ/mol H_2) is found to be lower than that for $LaMg_2NiH_7$ ($\Delta H_2 = -86.84$ kJ/mol H_2), suggesting $LaMg_2NiH_{4.5}$ may be a thermodynamically stable phase. As in previous studies, $LaMg_2NiH_{4.5}$ is also expected to be a stable intermediate hydride from the host compound $LaMg_2Ni$ to the full hydride $LaMg_2NiH_7$[17].

Electronic structure. To understand the bonding character of bulk $LaMg_2Ni$ and its hydrides $LaMg_2NiH_{4.5}$ and $LaMg_2NiH_7$, Fig. 3 shows their total and partial electronic density of states (TDOS and PDOS), where the Fermi level (E_F) is set at zero energy, and the four main bonding peaks of TDOS are marked with I, II, III and IV, respectively. For the host compound $LaMg_2Ni$ (Fig. 3a), the peak I has contribution from Mg *p* state. The peak

Systems	a	b	c	β	V (Å^3)	References
$LaMg_2Ni$	4.426 (4.227)	10.178 (10.303)	8.155 (8.360)	90^0 (90^0)	734.83 (728.02)	[15,20]
$LaMg_2NiH_{4.5}$	8.673 (8.602)	7.982 (7.937)	6.151 (6.114)	99.66^0 (99.53^0)	839.566 (823.334)	[17]
$LaMg_2NiH_7$	14.102 (13.979)	4.719 (4.703)	16.155 (16.025)	125.2^0 (125.24^0)	878.494 (860.39)	[15]
$LaMg_2Ni$–Co	4.207 (4.210)	10.105 (10.278)	8.340 (8.36)	90.0^0 (…)	733.158 (723.38)	[20]
$LaMg_2Ni$–Pd	4.363 (4.24)	10.258 (10.326)	8.259 (8.346)	90.02^0 (…)	739.291 (730.80)	[20]
$LaMg_2NiH_{4.5}$–Co	8.889 (…)	15.364 (…)	6.127 (…)	102.398^0 (…)	817.306 (…)	…
$LaMg_2NiH_{4.5}$–Pd	8.639 (…)	16.172 (…)	6.154 (…)	99.23^0 (…)	848.577 (…)	…
$LaMg_2NiH_7$–Co	14.028 (13.959)	4.701 (4.719)	16.151 (16.064)	125.27^0 (124.89^0)	869.052 (867.89)	[20]
$LaMg_2NiH_7$–Pd	14.148 (14.003)	4.728 (4.723)	16.177 (16.096)	125.16^0 (124.79^0)	884.62 (874.13)	[20]

Table 1. The optimized lattice constant and cell volume for $LaMg_2Ni$, $LaMg_2NiH_{4.5}$, $LaMg_2NiH_7$ and their corresponding Co- and Pd-containing compounds, in comparison with the available experimental/theoretical data. The numbers outside and inside the bracket correspond to our calculated results and the literature reports.

H-adsorbed $LaMg_2Ni$ (100) systems	E_{ads}	La–H			Ni–H		
		BO	BL	BO^s	BO	BL	BO^s
La–Ni bridge site	− 0.565	− 0.05	2.628 (1.878)	− 0.019	0.63	1.668 (1.877)	0.378
Top site of Ni	− 0.311	− 0.10	2.548	− 0.039	0.75	1.577 (1.875)	0.480
Top site of La	− 0.433	0.08	2.437 (1.875)	0.033	…	…	…

Table 2. The hydrogen adsorption energy (E_{ads}, in unit of eV), as well as the bond order (BO), the bond length (BL, in unit of Å) and the scaled bond order (BO^s, in unit of Å^{-1}) between La–H and Ni–H for H-adsorbed $LaMg_2Ni$ (100) systems. Numbers inside the bracket is the initial La–H and/or Ni–H distances.

II is dominated by La s state. The peak III is contributed by La *p* state. And the peak IV consists predominantly of Ni d and a few Ni *s*, Ni *p*, Mg *s*, Mg *p*, La *s*, La *p* and La *d* states. When $LaMg_2Ni$ is hydrogenated to form $LaMg_2NiH_{4.5}$ and $LaMg_2NiH_7$, the contributions of La, Mg and Ni electronic sates to the peaks I, II, III and IV remain unchanged, except H s state contributes to the peaks III and IV, as illustrated in Fig. 3b and c. Obviously, near the Fermi level (peak IV), the overlap electronic densities originated from La, Mg, Ni, or/and H atomic orbits suggest the atoms La, Mg, Ni, or/and H may interact to each other to form La–Mg, La–Ni, Mg–Ni, or/and La–H, Mg–H, Ni–H bonds. Furthermore, as shown for peak III, La p electrons overlap with H s electrons, also leading to the formation of La–H bond. Referring to the geometrical structure (Fig. 1), however, the distance between La–Mg in $LaMg_2Ni$, $LaMg_2NiH_{4.5}$ and $LaMg_2NiH_7$ (> 3.32 Å), and between La–Ni in $LaMg_2NiH_{4.5}$ and $LaMg_2NiH_7$ (> 3.09 Å) are so long that La atom is unlikely to interact with Mg and Ni atoms in these systems, thus, La–Mg bond in $LaMg_2Ni$, $LaMg_2NiH_{4.5}$ and $LaMg_2NiH_7$, and La–Ni bond in $LaMg_2NiH_{4.5}$ and $LaMg_2NiH_7$ can be ignored[31–33]. In addition, considering in peak IV the relatively high value of PDOS at Ni site, the Ni–H bond may have covalent character.

The charge density distribution is another intuitive way to investigate the bonding features. Figure 4 shows the results of charge density distribution for bulk $LaMg_2Ni$, $LaMg_2NiH_{4.5}$ and $LaMg_2NiH_7$ at La, Mg, Ni or/and H sites. In this figure, the contour lines are plotted from 0.03 to 0.3 electrons/Å^3. The shortest distances between La–Mg, La–Ni, Mg–Ni, or/and La–H, Mg–H, Ni–H obtained from Fig. 4 are listed in Table 3. Evidently, in $LaMg_2Ni$ system, Ni atom can interact with its neighboring Mg and La atoms to form Mg–Ni and La–Ni bonds respectively, as noted from the overlapping electrons between Mg–Ni and La–Ni in Fig. 4a. This formed La–Ni bond, however, tends to be broken from the intake of hydrogen, as the distance between La-Ni increases from 2.901 Å in $LaMg_2Ni$ to 4.407 Å in $LaMg_2NiH_{4.5}$ and 3.241 Å in $LaMg_2NiH_7$. The distance between La-Mg reaches to be 3.325 Å in $LaMg_2Ni$, 3.700 Å in $LaMg_2NiH_{4.5}$ and 3.677 Å in $LaMg_2NiH_7$, which is too long to form La-Mg bond. Additionally, as noted in Fig. 4b and c, a directional feature of charge density distribution around [NiH] group contributes to a covalent bond between Ni and H atoms, and this result is consistent with the findings of Miwa et al.[17]. Here, the bonding characteristics among La, Mg, Ni or/and H atoms described in charge density distribution (Fig. 4) are in good agreement with DOS analysis (Fig. 3).

To elucidate the bonding characteristics quantitatively, Mulliken population analysis is applied to bulk $LaMg_2Ni$, $LaMg_2NiH_{4.5}$ and $LaMg_2NiH_7$, including the average bond order (BO), average bond length (BL) and scaled bond order (BO^s), and the results are shown in Table 4. Here, BO^s, the average bond order (BO) per unit bond length (BL), is estimated using the formula $BO^s = BO/BL$, and can be used to evaluate the relative bonding strength between atoms[31,32,34–36]. A bond with positive BO^s is expected to be a covalent nature. Moreover, the higher the BO^s is, the stronger the bonding interaction is. The absent La–Ni bonds in $LaMg_2NiH_{4.5}$ and $LaMg_2NiH_7$, and La–Mg bonds in $LaMg_2Ni$, $LaMg_2NiH_{4.5}$ and $LaMg_2NiH_7$ (not shown in Table 4), and the presence of Mg–Ni, Ni–H, La–H and Mg-H bonds in studied systems are consistent with those described in Figs. 3 and 4. Evidently, with hydrogen absorption, the atomic interaction between Mg-Ni becomes weaker, but

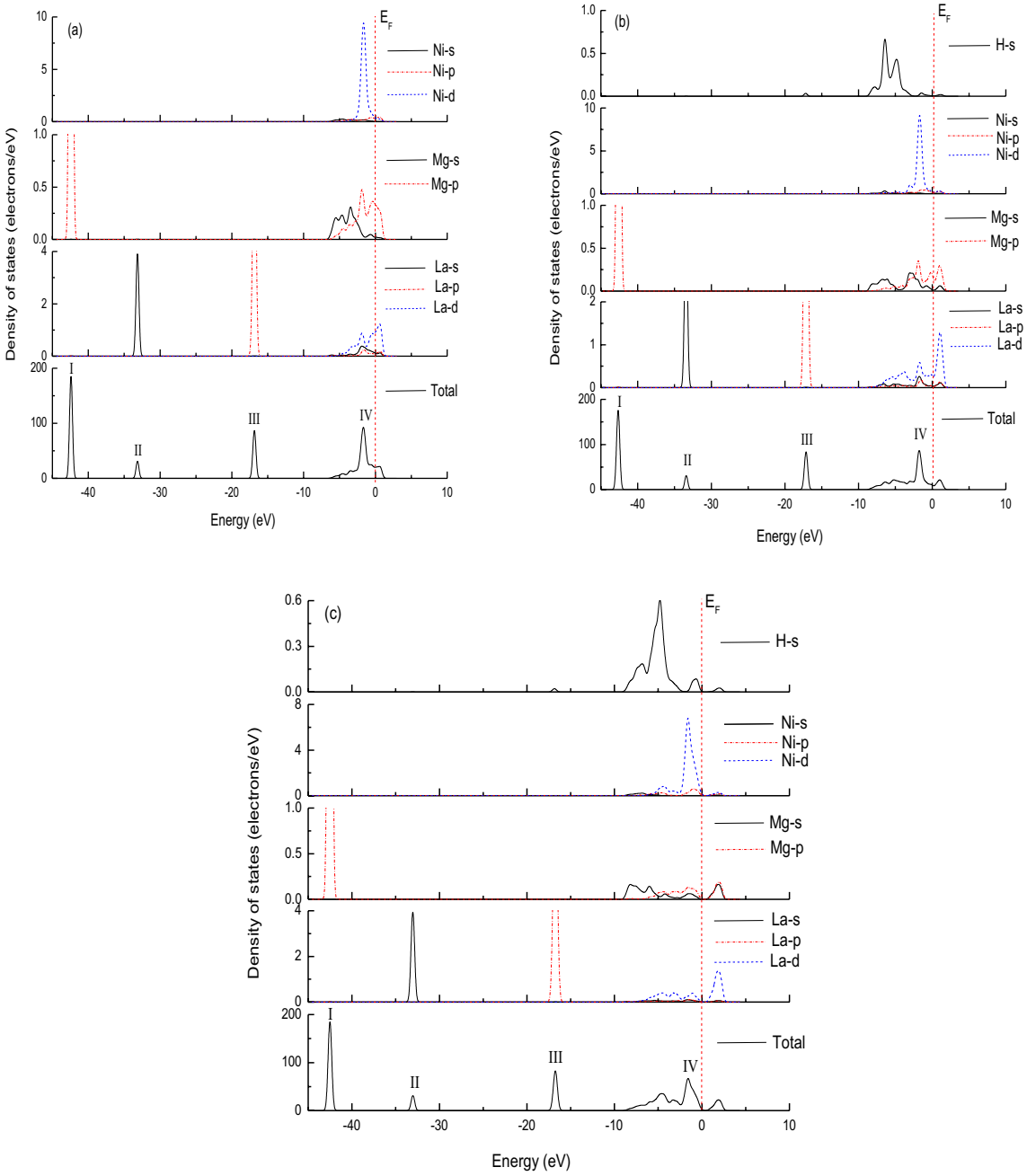

Figure 3. Total and partial density of states for studied compounds, (**a**) $LaMg_2Ni$, (**b**) $LaMg_2NiH_{4.5}$, (**c**) $LaMg_2NiH_7$. The Fermi level is set at zero energy and marked by the vertical dotted line.

between Ni–H becomes stronger, as noted from the decreased scaled bond order between Mg–Ni (BO^s_{Mg-Ni}) and the increased scaled bond order between Ni–H (BO^s_{Ni-H}) in Table 4. As in previous study, the Mg–Ni and Ni–H interactions are reported to affect directly the phase stability of binary Mg_2Ni intermetallic hydride based on the electronic structures of Mg_2Ni intermetallic hydride containing a variety of alloying elements[37]. In the present study, the impact of Mg–Ni and Ni–H interactions on the hydrogenation of ternary compound $LaMg_2Ni$ (the product of La and Mg_2Ni by ball milling) is discussed based on Mulliken population analysis of bulk $LaMg_2Ni$ and its hydrides $LaMg_2NiH_{4.5}$ and $LaMg_2NiH_7$ in comparison with corresponding Co- and Pd-containing compounds ($LaMg_2Ni$–Co, $LaMg_2NiH_{4.5}$–Co, $LaMg_2NiH_7$–Co, $LaMg_2Ni$–Pd, $LaMg_2NiH_{4.5}$–Pd and $LaMg_2NiH_7$–Pd, Table 4), because Co and Pd addition can drastically reduce the reaction time for $LaMg_2Ni$–H hydride formation[20]. It is found in Table 4 that that Pd, especially Co addition weakens the Mg-Ni interaction, as compared to corresponding Co- and Pd-free compounds. Moreover, with hydrogen uptake, the Mg–Ni interaction for Co- and Pd-containing compounds also gradually decreases, as the BO^s_{Mg-Ni} is eventually reduced by 74.6% ($LaMg_2Ni$–Co system) and 72.9% ($LaMg_2Ni$–Pd system). We believe that the decreased Mg–Ni interactions are beneficial for the improvement of hydrogenation properties of $LaMg_2Ni$. Referring to the Ni–H bonds, it is formed as the hydrogenation reaction to the intermediate hydride phase, and becomes stronger to the full hydride

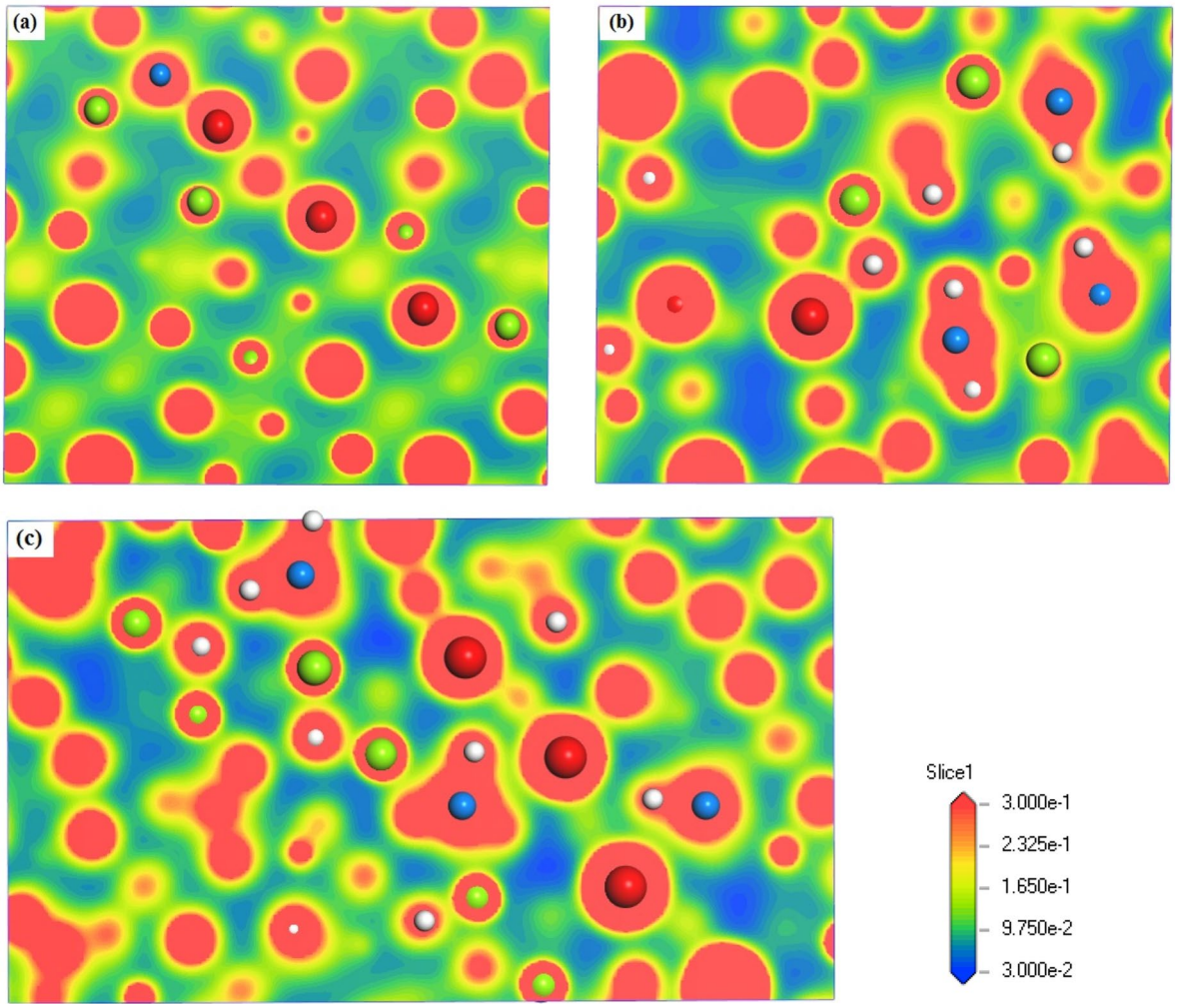

Figure 4. Charge density distribution for studied systems at La, Mg, Ni or/and H sites with the contour lines from 0.03 to 0.3 electrons/Å^3, (**a**) $LaMg_2Ni$, (**b**) $LaMg_2NiH_{4.5}$, (**c**) $LaMg_2NiH_7$. Red, green, blue and white spheres denote La, Mg, Ni and H atoms, respectively.

Systems	La–Mg	La–Ni	Mg–Ni	La–H	Mg–H	Ni–H
$LaMg_2Ni$	3.325	2.901	2.733	…	…	…
$LaMg_2NiH_{4.5}$	3.700	4.407	2.670	2.377	2.008	1.560
$LaMg_2NiH_7$	3.677	3.241	2.682	2.641	1.954	1.565

Table 3. The shortest distances between La–Mg, La–Ni, Mg–Ni, or/and La–H, Mg–H, Ni–H (in unit of Å) obtained from Charge density plots (Fig. 4) for $LaMg_2Ni$, $LaMg_2NiH_{4.5}$ and $LaMg_2NiH_7$.

phase, showing a covalent nature with the bond order between Ni–H being positive ($BO_{Ni-H} > 0$)[31,32,34,38]. Miwa et al.[17] and Sato et al.[19] had proposed that the intermediate hydride phase $LaMg_2NiH_{4.5}$ may play as precursor state for the following complex hydride $LaMg_2NiH_7$ formation as the Ni–H bonds in $LaMg_2NiH_{4.5}$ are essentially covalent nature similar to those in $LaMg_2NiH_7$, which subsequently provides the reduction of energy barrier for $LaMg_2Ni$ hydrogenation. According to this viewpoint, our intermediate hydrides $LaMg_2NiH_{4.5}$, $LaMg_2NiH_{4.5}$–Co and $LaMg_2NiH_{4.5}$–Pd with Ni–H covalent bonds may also act as precursor states for the following hydrogenation reaction to $LaMg_2NiH_7$, $LaMg_2NiH_7$–Co and $LaMg_2NiH_7$–Pd, respectively. In addition, it is worth noting that the introduction of Co and Pd not only hits growth in BO^s_{Ni-H} from 12.2% ($LaMg_2Ni$ system) to 3.95% ($LaMg_2Ni$–Co system) and 11.43% ($LaMg_2Ni$–Pd system) even in the case of increasing Ni–H interaction with more hydrogen absorption, but also weakens the Ni–H interactions at fully hydrogenated states, as the BO^s_{Ni-H} of 0.447 Å^{-1} for $LaMg_2NiH_7$–Co and 0.468 Å^{-1} for $LaMg_2NiH_7$–Pd are lower than that of 0.469 Å^{-1} for $LaMg_2NiH_7$. Interestingly, both the growth of BO^s_{Ni-H} from intermediate state to fully hydrogenated state and the BO^s_{Ni-H} at fully hydrogenated states decrease in the order of $LaMg_2Ni$ system (12.2%, 0.469 Å^{-1}) > Pd-containing $LaMg_2Ni$ system (11.43%, 0.468 Å^{-1}) > Co-containing $LaMg_2Ni$ system (3.95%, 0.447 Å^{-1}). This descending order is just

Systems	Mg–Ni			Ni–H			La–H			Mg–H		
	BO	BL	BO^s	BO	BL	BO^s	BO	BL	BO^s	BO	BL	BO^s
$LaMg_2Ni$	0.475	2.775	0.171	…	…	…	…	…	…	…	…	…
$LaMg_2NiH_{4.5}$	0.283	2.715	0.104	0.662	1.582	0.418	0.142	2.475	0.057	0.02	2.008	0.01
$LaMg_2NiH_7$	0.117	2.723	0.043	0.741	1.581	0.469	0.163	2.485	0.066	0.041	2.379	0.017
$LaMg_2Ni$–Co	0.441	2.795	0.158	…	…	…	…	…	…	…	…	…
$LaMg_2NiH_{4.5}$–Co	0.240	2.718	0.088	0.676	1.573	0.430	0.145	2.506	0.058	0.015	2.080	0.007
$LaMg_2NiH_7$–Co	0.110	2.722	0.040	0.724	1.619	0.447	0.159	2.485	0.064	0.045	2.275	0.020
$LaMg_2Ni$–Pd	0.476	2.794	0.170	…	…	…	…	…	…	…	…	…
$LaMg_2NiH_{4.5}$–Pd	0.279	2.719	0.103	0.663	1.580	0.420	0.152	2.475	0.061	0.022	2.120	0.010
$LaMg_2NiH_7$–Pd	0.126	2.724	0.046	0.740	1.582	0.468	0.173	2.486	0.070	0.049	2.335	0.021

Table 4. The average bond order (BO), average bond length (BL, in unit of Å) and scaled bond order (BO^s, in unit of $Å^{-1}$) between Mg–Ni, Ni–H, La–H and Mg–H for $LaMg_2Ni$, $LaMg_2NiH_{4.5}$ and $LaMg_2NiH_7$ and corresponding Co- and Pd-containing compounds $LaMg_2Ni$–Co, $LaMg_2NiH_{4.5}$–Co, $LaMg_2NiH_7$–Co, $LaMg_2Ni$–Pd, $LaMg_2NiH_{4.5}$–Pd and $LaMg_2NiH_7$–Pd according to Mulliken population analysis.

consistent with the reaction time for $LaMg_2Ni$–H formation, $LaMg_2Ni$ systems (7.5 h) > Pd-containing $LaMg_2Ni$ systems (3 h) > Co-containing $LaMg_2Ni$ systems (1.5 h)[20]. Thus, it is reasonable to conclude that the suppression of Ni–H interaction upon $LaMg_2Ni$ hydrogenation should accelerate $LaMg_2Ni$–H formation, and subsequently improve the hydrogenation performance of $LaMg_2Ni$. A similar example is found on Mg_2Ni system. Cu doping can accelerate Mg_2Ni hydride reaction followed with a reduction in Ni–H interaction in Mg_2NiH_4 hydride[39,40]. In the case of the La–H bonds formed upon hydrogenation of $LaMg_2Ni$, the La-H bond length (BL_{La-H}) in intermediate hydride $LaMg_2NiH_{4.5}$ (2.475 Å, Table 4) is very close to that in binary hydride LaH_3 (2.43 Å[16]). This characteristic is also embodied in Co- and Pd-containing $LaMg_2Ni$ systems with the BL_{La-H} of 2.506 Å in $LaMg_2NiH_{4.5}$–Co and 2.475 Å in $LaMg_2NiH_{4.5}$–Pd (Table 4). Pei et al.[8] had investigated the effect of La hydride compound on hydriding process of $LaMg_2Ni$, and showed that $LaMg_2Ni$ would decompose to LaH_3 during hydrogenation, and this La hydride compound was helpful to improve the hydrogen storage property of $LaMg_2Ni$ at low temperature. Many previous studies also verified that the La–H hydride could show good catalytic effect on hydriding reaction of $LaMg_2Ni$[11–13]. In our studies, we believe that the La–H interaction formed in $LaMg_2NiH_{4.5}$ may drive the formation of La–H hydride (such as LaH_3), and therefore effectively catalyze the fully hydrogenation reaction to $LaMg_2NiH_7$.

Figure 5 presents the band structure of bulk $LaMg_2Ni$, $LaMg_2NiH_{4.5}$ and $LaMg_2NiH_7$, where the Fermi level is set at zero energy; the band gap (E_g) characterized as the gap between the lowest energy of conduction band and the highest energy of valence band is shown in the inset of this figure. Obviously, for the host compound $LaMg_2Ni$, the valence and conduction bands overlap considerably and there is no band gap at the Fermi level, as illustrated in Fig. 5a. As a result, $LaMg_2Ni$ will show metallic property, which is consistent with the experimental report[16]. The characteristic of band structure for $LaMg_2Ni$ is also reflected on the intermediate hydride $LaMg_2NiH_{4.5}$, i.e., $LaMg_2NiH_{4.5}$ also has metallic nature (Fig. 5b). For the full hydride $LaMg_2NiH_7$, the band gap is predicted to be 0.821 eV using GGA method. This value is close to the literature finding of 0.9 eV (GGA value)[16], but is expected to be underestimated due to the strong on-site Coulomb interactions at d and f electronic states[41–43]. In general, a good agreement for band gap between theory and experiment can be obtained by adjusting the Hubbard U using GGA + U calculations[41–43]. In the present study, GGA + U calculation with different Hubbard U for La-5*d* and Ni-3*d* electrons has been employed on $LaMg_2NiH_7$, and found that the band gap of 1.454 eV at U = 3 eV for La and U = 6 eV for Ni is in the prediction by Yvon et al.[16]. Here, whatever $LaMg_2NiH_7$ has the band gap E_g = 0.821 eV (GGA value) or E_g = 1.454 eV (GGA + U value), this compound is expected to have insulator nature, and the result agrees well with the experimental finding[16]. In general, a high energy barrier associated with metal–insulator transition is expected during complex hydrogenation reaction from host metals to hydride nonmetals, because the local charge neutrality condition for complex hydrides becomes a strong constraint[17]. In our studies, because the host compound $LaMg_2Ni$ and the intermediate hydride $LaMg_2NiH_{4.5}$ are both metallic, the dehydrogenation reaction between them may be free from the energy barrier associated with the metal–insulator transition. In fact, the hydrogenation reaction of $LaMg_2Ni$ to $LaMg_2NiH_{4.5}$ process even at room temperature[17,19]. Once $LaMg_2Ni$ is hydrogenated to form $LaMg_2NiH_{4.5}$, this metallic intermediate hydride $LaMg_2NiH_{4.5}$ with Ni–H covalent bonds may act as precursor state for the following complex nonmetallic hydride $LaMg_2NiH_7$ formation (as described above). This will help to reduce the energy barrier for the hydrogenation reaction of $LaMg_2Ni$ to $LaMg_2NiH_7$ via intermediate phase $LaMg_2NiH_{4.5}$[17]. As in experiment, the hydrogenation reaction of $LaMg_2Ni$ to $LaMg_2NiH_7$ proceeds under moderate conditions (< 200 °C, < 0.8 MPa)[15]. A similar example can be found in YMn_2-H system. YMn_2 reacts with hydrogen to form YMn_2H_6 via metallic interstitial hydride $YMn_2H_{4.5}$ under relatively moderate conditions, at 423 K and 5 MPa H_2[44].

Hydrogen adsorption on surface. As described above, the formation of La–H bond and the suppression of Ni–H interactions are believed to favor for $LaMg_2Ni$–H formation. To further understand the impact of Ni–H and La–H on $LaMg_2Ni$ hydrogenation, hydrogen adsorption on $LaMg_2Ni$ (100) surface is investigated, with the

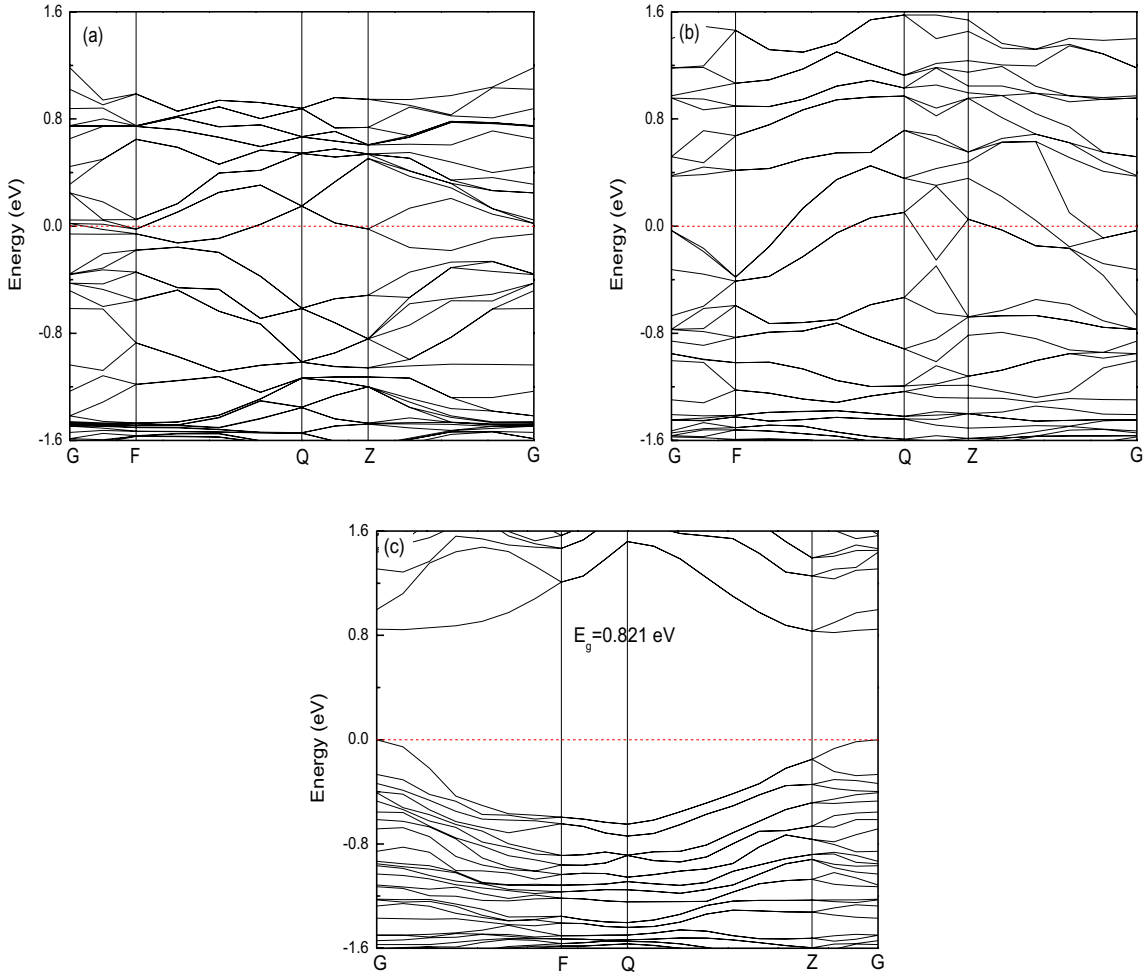

Figure 5. The band structure for studied compounds, (**a**) $LaMg_2Ni$, (**b**) $LaMg_2NiH_{4.5}$, (**c**) $LaMg_2NiH_7$.

initial positions of H on the bridge site of La–Ni atoms, the top site of La atom and the top site of Ni atom (Fig. 2). The hydrogen adsorption energy (E_{ads}) on the surface is expressed as following:

$$E_{ads} = E_{sur(100)/H} - E_{sur(100)} - E_H \quad (5)$$

where $E_{sur(100)/H}$ is the total energy of H-adsorbed systems, $E_{sur(100)}$ is the total energy of H-free systems, and E_H is the total energy of adsorbate H. E_H is estimated to be − 15.895 eV by the energy of H_2 (− 31.79 eV, as described above). The La-H and Ni–H bonding characteristics, including the bond order (BO), bond length (BL) and scaled bond order (BO^s), are studied by Mulliken population analysis. Table 2 lists the hydrogen adsorption energies (E_{ads}), as well as the bond order, the bond length, and the scaled bond order between La–H and Ni–H. As seen in Table 2, a presence of La–H and Ni–H bonds can be detected on all H-adsorbed $LaMg_2Ni$ (100) systems, except for an absence of Ni–H bond on the system with the initial H on the top site of La atom. And this absence may be ascribed to the long initial Ni–H distance (> 3.536 Å, Fig. 2b). H adsorption, on the one hand, leads the La–H distance to be close to that in LaH_3 hydride (2.43 Å[16]), especially for initial H adsorption on the top site of La atom (BL_{La-H} = 2.437 Å), suggesting the intake of H may drive the formation of La–H hydride upon $LaMg_2Ni$ hydrogenation. On the other hand, H adsorption results a shorter Ni–H distance due to Ni is attractive to H, as compared to its initial distance. The hydrogen adsorption energy E_{ads} is calculated to be − 0.565 eV (La-Ni bridge site), − 0.433 eV (Top site of La) and − 0.311 eV (Top site of Ni). In general, a negative E_{ads} is expected to be an exothermic reaction, and H atoms can adsorb on the surface stably. Moreover, an H atom with lower adsorption energy is easier to be adsorbed on the surfaces. Obviously, H atom considered here prefers to adsorb on the bridge site of La–Ni atoms to form La–H and Ni–H bonds simultaneously. Furthermore, the formed Ni–H bond interaction with BO^s_{Ni-H} = 0.378 $Å^{-1}$ is stronger than the formed La–H bond interaction with BO^s_{La-H} = -0.019 $Å^{-1}$. This suggests Ni atom is an active site on La–Mg–Ni alloy surface for H adsorption. Similar result is found on La–Ni systems[25,26]. It is worth noting that a H-adsorbed $LaMg_2Ni$ (100) system with relatively lower hydrogen absorption energy exhibits rather weaker Ni–H interactions, as noted E_{ads} = − 0.565 eV and BO^s_{Ni-H} = 0.378 $Å^{-1}$ for La–Ni bridge site system vs. E_{ads} = − 0.311 eV and BO^s_{Ni-H} = 0.480 $Å^{-1}$ for top site of Ni system in Table 2. We believe that the hydrogenation ability of $LaMg_2Ni$ should be improved if the Ni–H interactions are suppressed.

Conclusions

Electronic structures of $LaMg_2Ni$ and its hydrides (intermediate phase $LaMg_2NiH_{4.5}$ and fully hydrogenated phase $LaMg_2NiH_7$) were systematically investigated using first-principles density functional theory calculations, in comparison with those of corresponding Co- and Pd-doped compounds ($LaMg_2Ni$–Co, $LaMg_2NiH_{4.5}$–Co, $LaMg_2NiH_7$–Co, $LaMg_2Ni$–Pd, $LaMg_2NiH_{4.5}$–Pd and $LaMg_2NiH_7$–Pd). Hydrogenation behavior on $LaMg_2Ni$ (100) surface was also studied. Our studies aim at providing new insights into the hyrogenation of $LaMg_2Ni$. The results show the hydrogenation of $LaMg_2Ni$ to full hydride $LaMg_2NiH_7$ is energetically favorable, as the metallic intermediate hydride $LaMg_2NiH_{4.5}$ with Ni–H covalent bonds may act as the precursor state for $LaMg_2NiH_7$ formation. The suppression of Mg–Ni and Ni–H interactions coupled with the formation of La–H bond may improve the hydrogenation performance of $LaMg_2Ni$.

Received: 27 January 2020; Accepted: 8 July 2020
Published online: 22 July 2020

References

1. Dornheim, M. Tailoring reaction enthalpies of hydrides. In *Handbook of Hydrogen Storage* (ed. Hirscher, M.) (Wiley-VCH, New York, 2010).
2. Rönnebro, E. & Noréus, D. Surface sensitivity of Mg_2NiH_4 leading to a profound color change. *Appl. Surf. Sci.* **228**, 115–119 (2004).
3. Shao, H. Y., Liu, T., Wang, Y. T., Xu, H. R. & Li, X. G. Preparation of Mg-based hydrogen storage materials from metal nanoparticles. *J. Alloys. Compd.* **465**, 527–533 (2008).
4. Rusman, N. A. A. & Dahari, M. A review on the current progress of metal hydrides material for solid-state hydrogen storage applications. *Int. J. Hydrogen Energy* **41**, 12108–12126 (2016).
5. Tan, Z. H. *et al.* Hydrogen generation by hydrolysis of Mg–Mg_2Si composite and enhanced kinetics performance from introducing of $MgCl_2$ and Si. *Int. J. Hydrogen. Energy* **43**, 2903–2912 (2018).
6. Reilly, J. J. & Wiswall, R. H. Reaction of hydrogen with alloys of magnesium and nickel and the formation of Mg_2NiH_4. *Inorg. Chem.* **7**, 2254–2256 (1968).
7. Vyas, D. *et al.* Effect of Cu catalyst on the hydrogenation and thermodynamic properties of Mg_2Ni. *Int. J. Hydrogen Energy* **37**, 3755–3760 (2012).
8. Pei, L. C. *et al.* Effect of La hydride compound on hydriding process of Mg_2Ni phase in $LaMg_2Ni$ alloy. *Chin. J. Inorg. Chem.* **28**, 1489–1494 (2012).
9. Hongo, T. *et al.* Significance of grain boundaries and stacking faults on hydrogen storage properties of Mg_2Ni intermetallics processed by high-pressure torsion. *Acta Mater.* **92**, 46–54 (2015).
10. Wei, P. F. *et al.* Intrinsic alterations in the hydrogen desorption of Mg_2NiH_4 by solid dissolution of titanium. *Dalton Trans.* **47**, 8418–8426 (2018).
11. Ouyang, L. Z., Yao, L., Dong, H. W., Li, L. Q. & Zhu, M. Hydrogen storage properties of $LaMg_2Ni$ prepared by induction melting. *J. Alloys Compd.* **485**, 507–509 (2009).
12. Zhao, X., Han, S. M., Zhu, X. L., Liu, B. Z. & Liu, Y. Q. Investigations on hydrogen storage properties of Mg_2Ni+xwt% $LaMg_2Ni$ (x=0, 10, 20, 30) composites. *J. Solid. State. Chem.* **190**, 68–72 (2012).
13. Pei, L. C. *et al.* Hydrogen storage properties and phase structures of RMg_2Ni (R=La, Ce, Pr, Nd) alloys. *Mater. Sci. Eng. B* **177**, 1589–1595 (2012).
14. Xie, D. H., Li, P., Zeng, C. X., Sun, J. W. & Qu, X. H. Effect of substitution of Nd for Mg on the hydrogen storage properties of Mg_2Ni alloy. *J. Alloys. Compd.* **478**, 96–102 (2009).
15. Renaudin, G., Guénée, L. & Yvon, K. $LaMg_2NiH_7$, a novel quaternary metal hydride containing tetrahedral $[NiH_4]^{4-}$ complexes and hydride anions. *J. Alloys. Compd.* **350**, 145–150 (2003).
16. Yvon, K., Renaudin, G., Wei, C. M. & Chou, M. Y. Hydrogenation-induced insulating state in the intermetallic compound $LaMg_2Ni$. *Phys. Rev. Lett.* **94**, 066403 (2005).
17. Miwa, K. *et al.* Metallic intermediate hydride phase of $LaMg_2Ni$ with Ni-H covalent bonding: precursor state for complex hydride formation. *J. Phys. Chem. C* **120**, 5926–5931 (2016).
18. Sato, T. *et al.* In-situ powder neutron diffraction study on the formation process of $LaMg_2NiH_7$. *Int. J. Hydrogen Energy* **42**, 22449–22453 (2017).
19. Sato, T., Ramirez-Cuesta, A. J., Daemen, L. L., Cheng, Y. & Orimo, S. I. Evidence of intermediate hydrogen states in the formation of a complex hydride. *Inorg. Chem.* **57**, 867–872 (2018).
20. Teresiak, A., Uhlemann, M., Thomas, J., Eckert, J. & Gebert, A. Influence of Co and Pd on the formation of nanostructured $LaMg_2Ni$ and its hydrogen reactivity. *J. Alloys Compd.* **582**, 647–658 (2014).
21. Segall, M. D. *et al.* First-principles simulation: ideas, illustrations and the CASTEP code. *J. Phys. Condens. Matter* **14**, 2717–2744 (2002).
22. Perdew, J. P. & Wang, Y. Accurate and simple analytic representation of the electron-gas correlation energy. *Phys. Rev. B* **45**, 13244–13249 (1992).
23. Fischer, T. & Almlöf, J. General methods for geometry and wave function optimization. *J. Phys. Chem.* **96**, 9768–9774 (1992).
24. Wallace, W. E., Karllcek, R. F. & Imamura, H. Mechanism of hydrogen absorption by $LaNi_5$. *J. Phys. Chem.* **83**, 1708–1712 (1979).
25. Shi, S. Q., Ouyang, C. Y. & Lei, M. S. Crystal structure and electrochemical characteristics of non-AB_5 type La-Ni system alloys. *J. Power Sources* **164**, 911–915 (2007).
26. Han, S. *et al.* Experimental and theoretical investigation of the cycle durability against CO and degradation mechanism of the $LaNi_5$ hydrogen storage alloy. *J. Alloys Compd.* **446–447**, 208–211 (2007).
27. Lan, Z. Q., Jiang, W. Q., Bai, J. D. & Guo, J. The first-principles investigation on the electronic structure and mechanism of $LiH+NH_3 \rightarrow LiNH_2+H_2$ reaction. *Int. J. Hydrogen Energy* **37**, 18937–18943 (2012).
28. Wang, H. Y., Zhang, N., Wang, C. & Jiang, Q. C. First-principles study of the generalized stacking fault energy in Mg-3Al-3Sn alloy. *Scripta. Mater.* **65**, 723–726 (2011).
29. Fukai ,Y. The metal-hydrogen system. In *Springer Series in Material Science*, vol. 21. (Springer-Verleg, Berlin, 1993).
30. Zhang, J., Sun, L. Q., Zhou, Y. C. & Peng, P. Dehydrogenation thermodynamics of magnesium hydride doped with transition metals: experimental and theoretical studies. *Comp. Mater. Sci.* **98**, 211–219 (2015).
31. Jiang, W. Q. & Cao, S. L. Effect of Al on the dehydrogenation of $LiBH_4$ from first-principles calculations. *Int. J. Hydrogen Energy* **42**, 6181–6188 (2017).
32. Mo, X. H. & Jiang, W. Q. Dehydrogenation properties of $LiBH_4$ modified by Mg from first-principles calculations. *J. Alloys Compd.* **735**, 668–676 (2018).
33. Huang, Z. N. *et al.* Synergistic effects of Mg and N cosubstitution on enhanced dehydrogenation properties of $LiBH_4$: a first-principles study. *J. Phys. Chem. C* **123**, 1550–1558 (2019).

34. Mo, X. H. & Jiang, W. Q. A comparative study on dehydrogenation of Mg-doped $LiBH_4$ and $Li_2B_{12}H_{12}$ from first-principle calculations. *Comp. Mater. Sci.* **154**, 187–193 (2018).
35. Huang, R. Z., Wang, Y. M., Wang, J. Y. & Zhou, Y. C. First-principles investigations of the stability and electronic structure of ZrV2Hx (x=05, 1, 2, 3, 4, 6 and 7). *Acta Mater.* **52**, 3499–3506 (2004).
36. Zhang, R. J., Wang, Y. M., Chen, D. M., Yang, R. & Yang, K. First-principles calculations of $LaNi_4Al$-H solid solution and hydrides. *Acta Mater.* **54**, 465–472 (2006).
37. Takahashi, Y., Yukawa, H. & Morinaga, M. Alloying effects on the electronic structure of Mg_2Ni intermetallic hydride. *J. Alloys Compd.* **242**, 98–107 (1996).
38. Wang, H. P. *et al.* Density function study of H_2 adsorption on LiB (010) surface. *Phys. B* **405**, 1792–1795 (2010).
39. Zhang, J. The structures and dehydrogenation properties of Cu alloying Mg_2NiH_4 hydrogen storage system. *Mater. Rep.* **25**, 84–87 (2011).
40. Zhang, J., Zhou, D. W., Peng, P. & Liu, J. S. First-principles plane-wave pseudopotential method calculations for Cu alloying Mg_2Ni hydride. *Mater Sci.* **26**, 681–691 (2008).
41. Feng, J. *et al.* Electronic structure, mechanical properties and thermal conductivity of $Ln_2Zr_2O_7$ (Ln=La, Pr, Nd, Sm, Eu and Gd) pyrochlore. *Acta Mater.* **59**, 1742–1760 (2011).
42. Shi, S. Q. *et al.* Multi-scale computation methods: their applications in lithium-ion battery research and development. *Chin. Phys. B* **25**, 018212 (2016).
43. Tumanov, N. A. *et al.* High-pressure study of $Mn(BH_4)_2$ reveals a stable polymorph with high hydrogen density. *Chem. Mater.* **28**, 274–283 (2016).
44. Matsuo, M. *et al.* First-principles studies of complex hydride YMn2H6 and its synthesis from metal hydride YMn2H45. *Appl. Phys. Lett.* **98**, 221908 (2011).

Acknowledgments

This work was supported by the National Natural Science Foundation of China (51661002, 51401056), the Natural Science Foundation of Guangxi (2018GXNSFAA138189, 2015GXNSFAA139259), and the high-performance computing platform of Guangxi University.

Author contributions

W.Q.J. directed the total paper and theoretical works. W.Q.J. and Y.J.C. put forward the idea and wrote the paper. X.H.M. analyzed the data and helped with improving the manuscript. X.L.L. created the models and figures. All authors reviewed the manuscript.

Competing interests

The authors declare no competing interests.

Additional information

Correspondence and requests for materials should be addressed to W.J.

Reprints and permissions information is available at www.nature.com/reprints.

Publisher's note Springer Nature remains neutral with regard to jurisdictional claims in published maps and institutional affiliations.